Supporting Information

Unraveling the high-activity nature of Fe-N-C electrocatalysts for oxygen reduction reaction: the extraordinary synergy between Fe-N_4 and Fe_4N

Table of contents

1. Material Synthesis

Principle and tactics

First, NaCl crystals with a face-centered cubic (FCC) structure were synthesized, and serve as templates for preparation of the 3D porous carbon networks, inhibiting the agglomeration of Fe-based nanoparticles. Second, D(+)-glucosamine hydrochloride ($C_6H_{13}NO_5$•HCl) was chosen as the precursor since it can be homogeneously distributed in $FeCl_3$ solution due to the strong interactions between the functional groups of $C_6H_{13}NO_5$•HCl and ferric ion. Third, dicyandiamide ($C_2H_4N_4$) was further added into the solution under stirring. During the further pyrolysis process, $C_2H_4N_4$ gradually decomposed with simultaneous release of a large amount of carbon nitrogen species (e.g. $C_2N_2^+$, $C_3N_2^+$, $C_3N_3^+$).[1] By reacting with $C_6H_{13}NO_5$•HCl and its further evolvement, 3D N-doped interconnected carbon networks was formed. Finally, the NaCl templates was removed.

2. Theoretical Section

Reaction mechanism

To understand the nature of the high oxygen reduction reaction (ORR) activity of Fe_4N

supported Fe-N_4 systems, we further performed density functional theory (DFT) calculations to investigate the free energetics of the ORR reaction mechanism. The pathways on Fe_4N supported Fe-N_4 systems were calculated in detail according to electrochemical framework developed by Nørskov and co-workers.[2] For the ORR in an alkaline electrolyte (pH=13), as H_2O/H_3O^+ may act as the proton donor, the overall reaction scheme of the ORR can be expressed as:

$$O_2+2H_2O+4e^- \leftrightarrow 4OH^-$$

The ORR can proceed through the following elementary steps usually employed to investigate the electrocatalysis of the ORR on various materials:

$$O_2(g) + H_2O(l) + e^- + * \rightarrow OOH^* + OH^- \quad (1)$$

$$OOH^* + e^- \rightarrow O^* + OH^- \quad (2)$$

$$O^* + H_2O\ (l) + e^- \rightarrow OH^* + OH^- \quad (3)$$

$$OH^* + e^- \rightarrow OH^- + * \quad (4)$$

where * stands for an active site on the catalytic surface, (l) and (g) refer to liquid and gas phases, respectively.

Structure optimization and adsorption

For comparison, the catalytic activity of free Fe-N_4 moieties, bare Fe_4N and Fe_4N supported Fe-N_4 moieties were all investigated. In Fe_4N crystals, the exposed surface are either Fe or N atom. Considering all the possible atoms configuration in real catalyst, four models of Fe_4N were drafted: Fe_4N(001)-Fe, Fe_4N(001)-N; Fe_4N(111)-Fe; Fe_4N(111)-FeN (Fig. S12). Moreover, for the Fe_4N supported Fe-N_4 moieties case, four possible structures were considered and built: Fe_4N(001)-FeN supported Fe-N_4; Fe_4N(001)-Fe supported Fe-N_4; Fe_4N(111)-Fe supported Fe-N_4; Fe_4N(111)-FeN supported Fe-N_4 (Fig. S13). In order to demonstrate the stability and synergistic effect of these catalysts models, we calculated the interaction energy between the Fe_4N and Fe or FeN. The interaction energies between Fe_4N and Fe or FeN are -1.78 eV, 1.37 eV, 3.94 eV and 3.13 eV for Fe_4N(001)-Fe, Fe_4N(001)-N; Fe_4N(111)-Fe; Fe_4N(111)-FeN, respectively. So, all the Fe_4N supported structures are stable. To demonstrate the stability and synergistic effect of these catalysts models, we calculated the interaction

energy between the Fe_4N and Fe or FeN. The interaction energies between Fe_4N and Fe or FeN are -1.78 eV, 1.37 eV, 3.94 eV and 3.13 eV for Fe_4N(001)-Fe, Fe_4N(001)-N; Fe_4N(111)-Fe; Fe_4N(111)-FeN, respectively. Thus, all the Fe_4N supported structures are stable. The free Fe-N_4 model can be seen in Fig. S14.

To examine the catalytic activity, we calculated the adsorption energies of O_2, O, OH, and OOH. Fig. S15 shows the adsorption structures of O_2, O, OH, and OOH on supported- or free Fe-N_4 moieties, the detail calculated free energy values of which could refer to Table S4.

Reaction free energy calculation

For proton-transfer steps, reaction free energies are generally regarded as the activation barriers. Since the transfer of a solvated proton to adsorbed OH^- show a negligible overbarrier, it suggests that the proton transfer is downhill in energy.[3] This approximation may result in slight overestimation of activity for a given proton-transfer elementary step, but can still qualitatively represent the relative energetic ordering of the various proton-transfer elementary steps. Thus, we use reactions (1)-(4) to derive the thermochemistry for ORR.

The chemical potential of each adsorbate is defined as:

$$\mu = E + E_{ZPE} - T \times S$$

where the E is the total energy obtained from DFT calculations, E_{ZPE} is zero-point energy and S is the entropy at 298 K. To obtain the reaction free energy of each elementary step of the ORR, we calculated the adsorption free energy of O^*, OH^*, and OOH^*. Since it is difficult to obtain the exact free energy of OOH, O, and OH radicals in the electrolyte solution, the adsorption free energy ΔG_{O^*}, ΔG_{OH^*}, and ΔG_{OOH^*}, are relative to the free energy of appropriate stoichiometric amounts of H_2O (g) and H_2 (g) , defined as follows:

(1) $\Delta G_{O^*} = \Delta G\left(H_2O(g) + {}^* \rightarrow O^* + H_2(g)\right) = \mu_{O^*} + \mu_{H_2} - \mu_{H_2O} - \mu^*$

$$= \left(E_{O^*} + E_{H_2} - E_{H_2O} - E_*\right) + \left(E_{ZPE(O^*)} + E_{ZPE(H_2)} - E_{ZPE(H_2O) - E_{ZPE(^*)}}\right) - T \times (S_{O^*} + S_{H_2} - S_{H_2O} - S_*)$$

(2) $\Delta G_{OH^*} = \Delta G\left(H_2O(g) + {}^* \rightarrow OH^* + 1/2\, H_2(g)\right) = \mu_{OH^*} + 1/2\, \mu_{H_2} - \mu_{H_2O} - \mu^*$

$= \left(E_{OH^*} + 1/2\, E_{H_2} - E_{H_2O} - E_*\right) + \left(E_{ZPE(OH^*)} + 1/2\, E_{ZPE(H_2)} - E_{ZPE(H_2O) - E_{ZPE(^*)}}\right)$

$- T \times (S_{OH^*} + 1/2\, S_{H_2} - S_{H_2O} - S_*)$

(3) $\Delta G_{OOH^*} = \Delta G\left(2H_2O(g) + {}^* \rightarrow OOH^* + 3/2\, H_2(g)\right) = \mu_{OOH^*} + 3/2\, \mu_{H_2} - 2\mu_{H_2O} - \mu^*$

$= \left(E_{OOH^*} + 3/2\, E_{H_2} - 2E_{H_2O} - E_*\right) + \left(E_{ZPE(OOH^*)} + 3/2\, E_{ZPE(H_2)} - 2E_{ZPE(H_2O) - E_{ZPE(^*)}}\right)$

$- T \times (S_{OOH^*} + 3/2\, S_{H_2} - 2S_{H_2O} - S_*)$

Here, the asterisk (*) indicates an adsorption site. Entropy values of gaseous molecules are taken from the standard tables in the Physical Chemistry text book,[4] while the entropies of adsorbate and adsorption site are negligible. The zero-point energy for each adsorbate and free molecules can be obtained from the vibration frequency calculation, while the zero-point energy of adsorption site is negligible. All the E_{ZPE} and S results are summarized in Table S5.

For each elementary step, the Gibbs reaction free energy ΔG is defined as the difference between free energies of the initial and final states, and is given by the following expression:

$$\Delta G = \Delta E + \Delta ZPE - T\Delta S + \Delta G_U + \Delta G_{pH}$$

where ΔE is the reaction energy of reactant and product molecules adsorbed on catalyst surface, obtained from DFT calculations; ΔZPE and ΔS are the change in zero point energies and entropy during the reaction. The bias effect on the free energy of each initial, intermediate and final state involving electrons transfer in the electrode is also taken into account by shifting the energy of the state by $\Delta G_U = -neU$, where U is the electrode applied potential, e is the transferred charge and n is the number of proton–electron transferred pairs. The change of free energy owing to the effect of pH value of the electrolyte is considered by the correction of H^+ ions concentration ($[H^+]$) dependence of the entropy, $\Delta G_{pH} = -k_B T \ln[H^+] = pH \times k_B T \ln 10$, where k_B is the Boltzmann constant and T is the temperature. Given the fact that the high-spin ground state of the oxygen molecule is poorly described in DFT calculations, the free energy of the O_2 molecule was determined by $G_{O_2}(g) = 2G_{H_2O}(l) - 2G_{H_2} + 4 \times 1.23(eV)$. The free energy of OH^- was derived as $G_{OH^-} = G_{H_2O}(l) - 2G_{H^+}$. The

free energy for gas phased water was calculated at 0.035 bars because this is the equilibrium pressure in contact with liquid water at 298 K. The free energy of gas phase water at these conditions is equal to the free energy of liquid water.

The reaction free energy of (1)-(4) for the ORR can be determined from the following equations:

(1) $\boldsymbol{O_2(g) + H_2O(l) + e^- \rightarrow OOH^* + OH^-}$

$$\Delta G_1 = \mu_{OOH^*} + \mu_{OH^-} - \mu_{H_2O} - \mu_* - \mu_{O_2} - \mu_{e^-}$$

$$= \mu_{OOH^*} + \left(\mu_{H_2O} - \mu_{H^+}\right) - \mu_{H_2O} - \mu_* - \left(2\mu_{H_2O} - 2\mu_{H_2} + 4 \times 1.23\right) - \mu_{e^-}$$

$$= \mu_{OOH^*} + 3/2 \times \mu_{OOH^*} - 2\mu_{H_2O} - \mu_* - 4.92$$

$$= \Delta G_{OOH^*} - 4.92$$

(2) $\boldsymbol{OOH^* + e^- \rightarrow O^* + OH^-}$

$$\Delta G_2 = \mu_{O^*} + \mu_{OH^-} - \mu_{OOH^*} - \mu_{e^-}$$

$$= \mu_{O^*} + \left(\mu_{H_2O} - \mu_{H^+}\right) - \mu_{OOH^*} - \mu_{e^-}$$

$$= \mu_{O^*} + \mu_{H_2O} - 1/2\,\mu_{H_2} - \mu_{OOH^*}$$

$$= (\mu_{O^*} + \mu_{H_2} - \mu_{H_2O} - \mu_*) - (\mu_{OOH^*} + 3/2\,\mu_{H_2} - 2\mu_{H_2O} - \mu_*)$$

$$= \Delta G_{O^*} - \Delta G_{OOH^*}$$

(3) $\boldsymbol{O^* + H_2O + e^- \rightarrow OH^* + OH^-}$

$$\Delta G_3 = \mu_{OH^*} + \mu_{OH^-} - \mu_{O^*} - \mu_{H_2O} - \mu_{e^-}$$

$$= \mu_{OH^*} + \left(\mu_{H_2O} - \mu_{H^+}\right) - \mu_{O^*} - \mu_{H_2O} - \mu_{e^-}$$

$$= \mu_{OH^*} - 1/2\,\mu_{H_2} - \mu_{O^*}$$

$$= (\mu_{OH^*} + 1/2\,\mu_{H_2} - \mu_{H_2O} - \mu_*) - (\mu_{O^*} + \mu_{H_2} - \mu_{H_2O} - \mu_*)$$

$$= \Delta G_{OH^*} - \Delta G_{O^*}$$

(4) $\boldsymbol{OH^* + e^- \rightarrow OH^- + ^*}$

$$\Delta G_4 = \mu_{OH^-} + \mu^* - \mu_{OH^*} - \mu_{e^-}$$

$$= \left(\mu_{H_2O} - \mu_{H^+}\right) + \mu^* - \mu_{OH^*} - \mu_{e^-}$$

$$= \mu_{H_2O} - 1/2\,\mu_{H_2} + \mu^* - \mu_{OH^*}$$

$$= -(\mu_{OH^*} + 1/2\,\mu_{H_2} - \mu_{H_2O} - \mu^*)$$

$$= -\Delta G_{OH^*}$$

For the ORR, the onset potential is calculated by

$$U^{onset}_{ORR} = -\max\{\Delta G1, \Delta G2, \Delta G3, \Delta G4\}$$

3. Supporting Figures and Tables

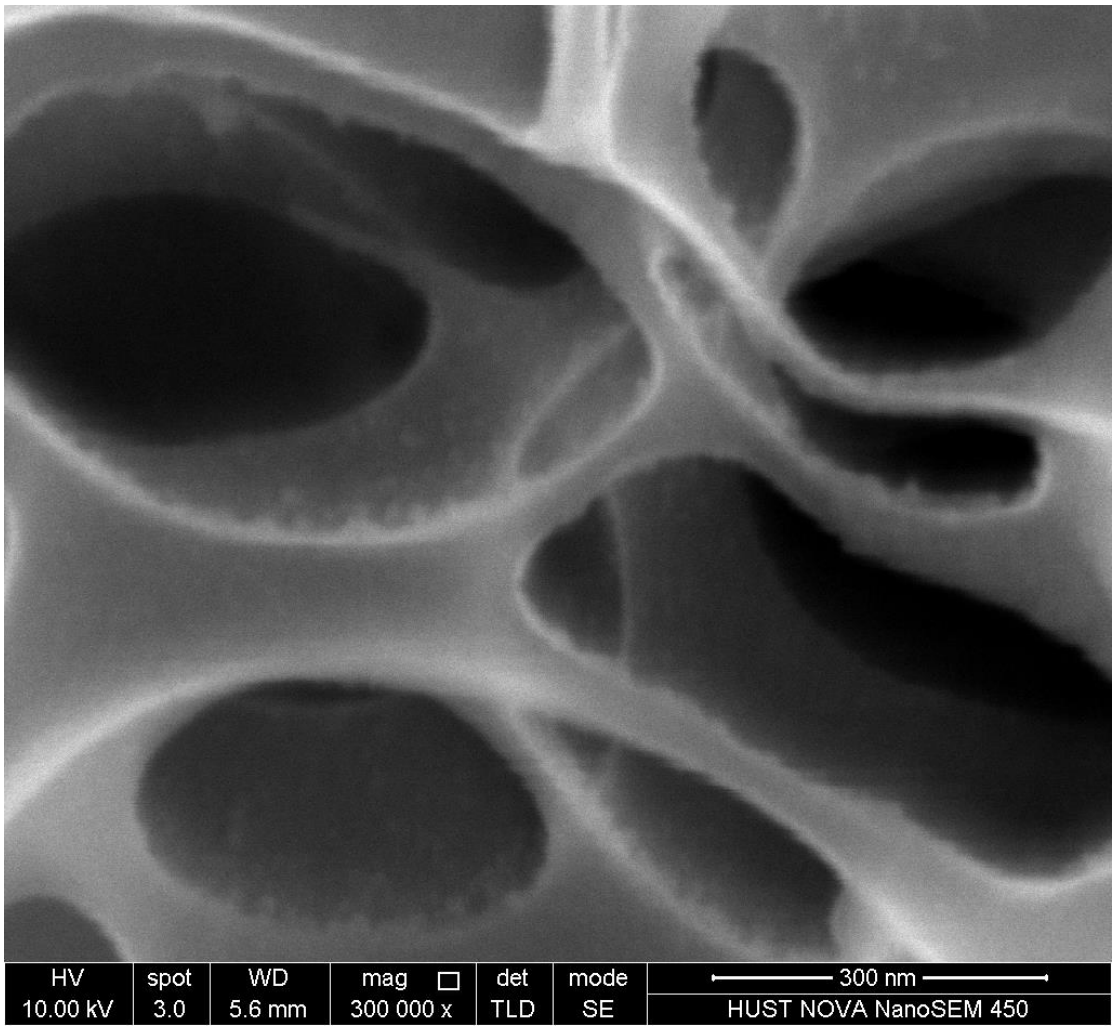

Fig. S1 Enlarged SEM image of FeNCNs-800.

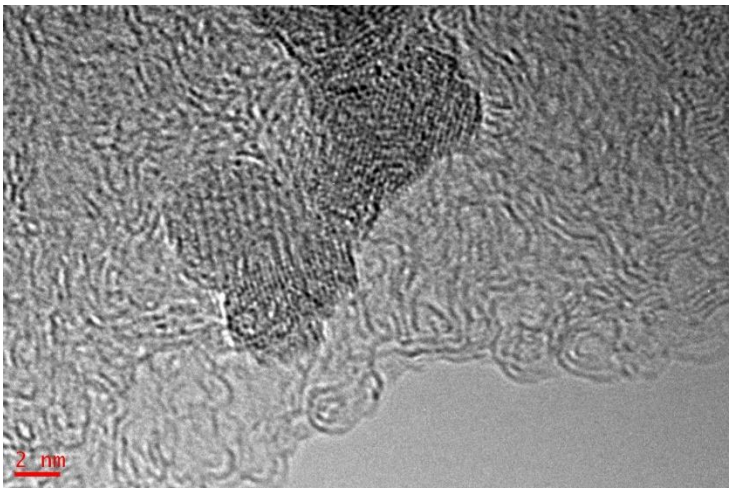

Fig. S2 HRTEM image of FeNCNs-800.

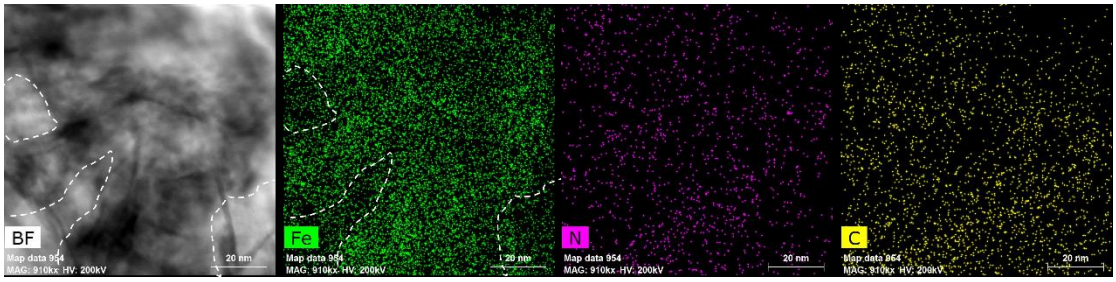

Fig. S3 EDS elemental mapping images of FeNCNs-800 in larger magnification.

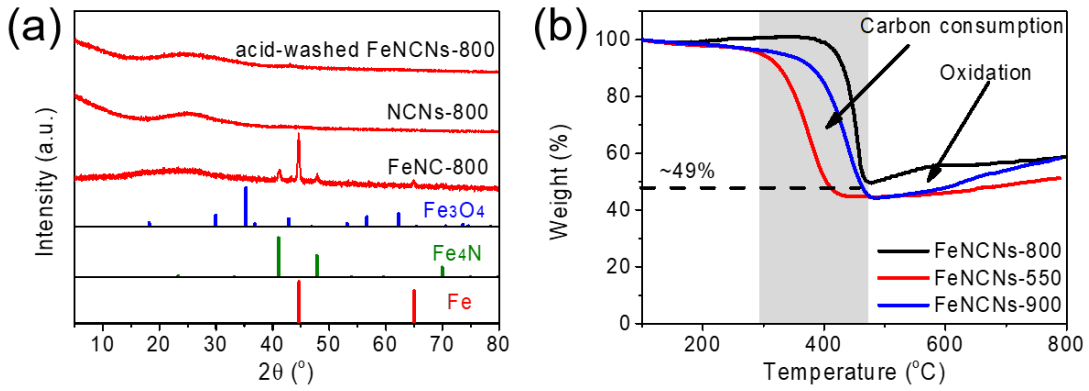

Fig. S4 (a) XRD patterns of acid-washed FeNCNs-800, NCNs-800 and FeNC-800, (b) TGA results of FeNCNs-550, FeNCNs-800, and FeNCNs-900.

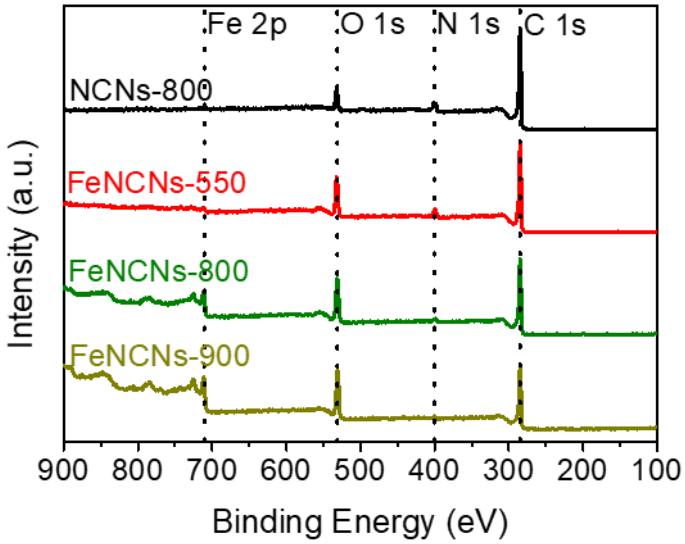

Fig. S5 XPS survey of NCNs-800, FeNCNs-550, FeNCNs-800, and FeNCNs-900.

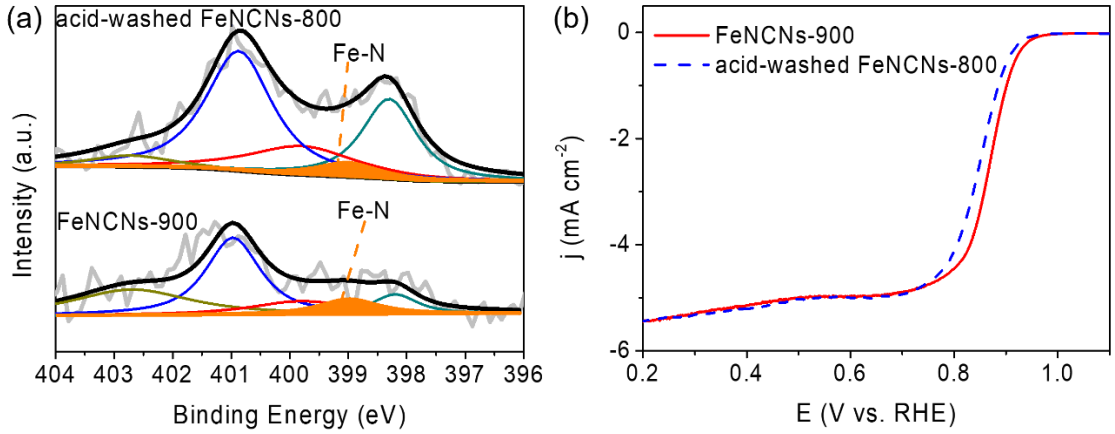

Fig. S6 (a) XPS N 1s spectra and (b) ORR polarization curves of FeNCNs-900 and acid-washed FeNCNs-800.

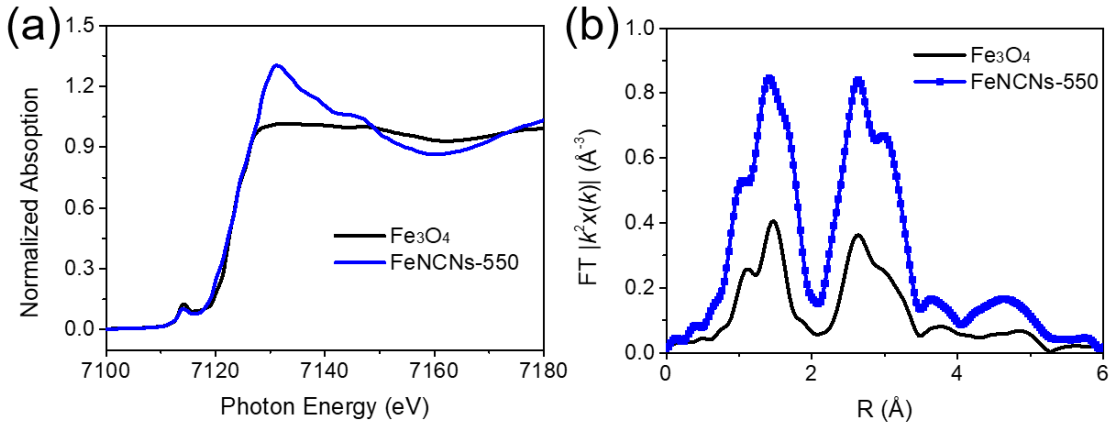

Fig. S7 (a) Fe *k*-edge XANES spectra of FeNCNs-550, and Fe_3O_4, (b) the Fourier transforms of k^2-weighted $x(k)$-function of the EXAFS spectra for FeNCNs-550, and Fe_3O_4.

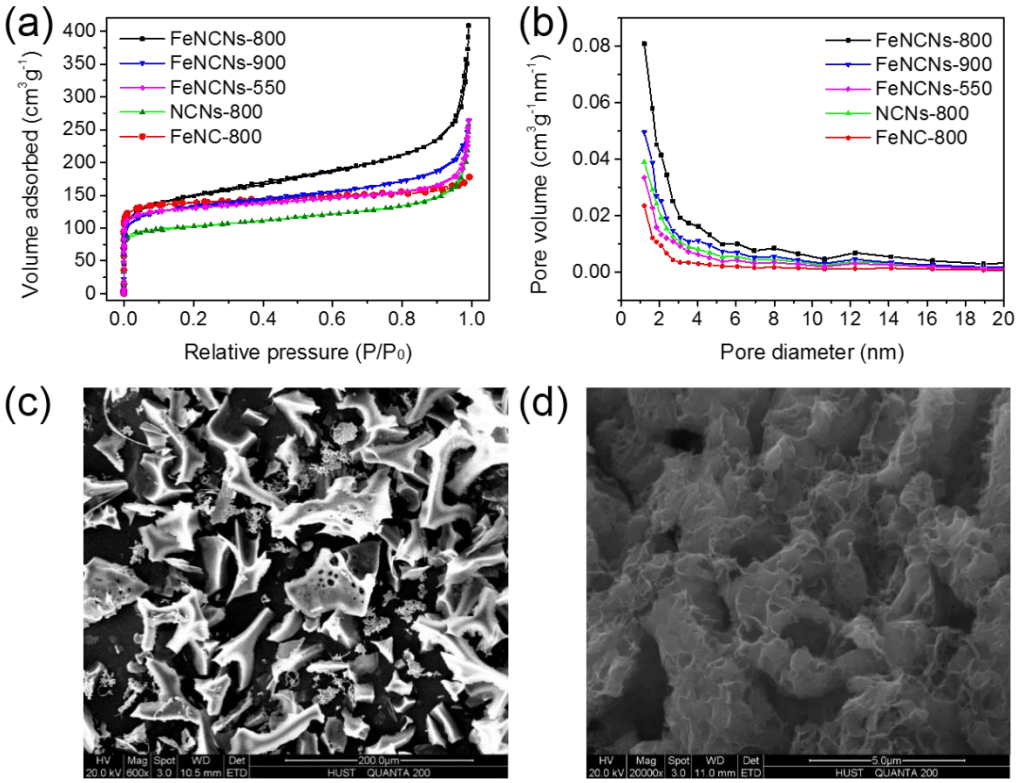

Fig. S8 (a) The N_2 adsorption-desorption isotherms and (b) corresponding pore size distribution of FeNCNs-800, FeNCNs-900, FeNCNs-550, NCNs-800 and FeNC-800. SEM images of (c) the FeNC-800 and (d) the synthesized product before removing NaCl.

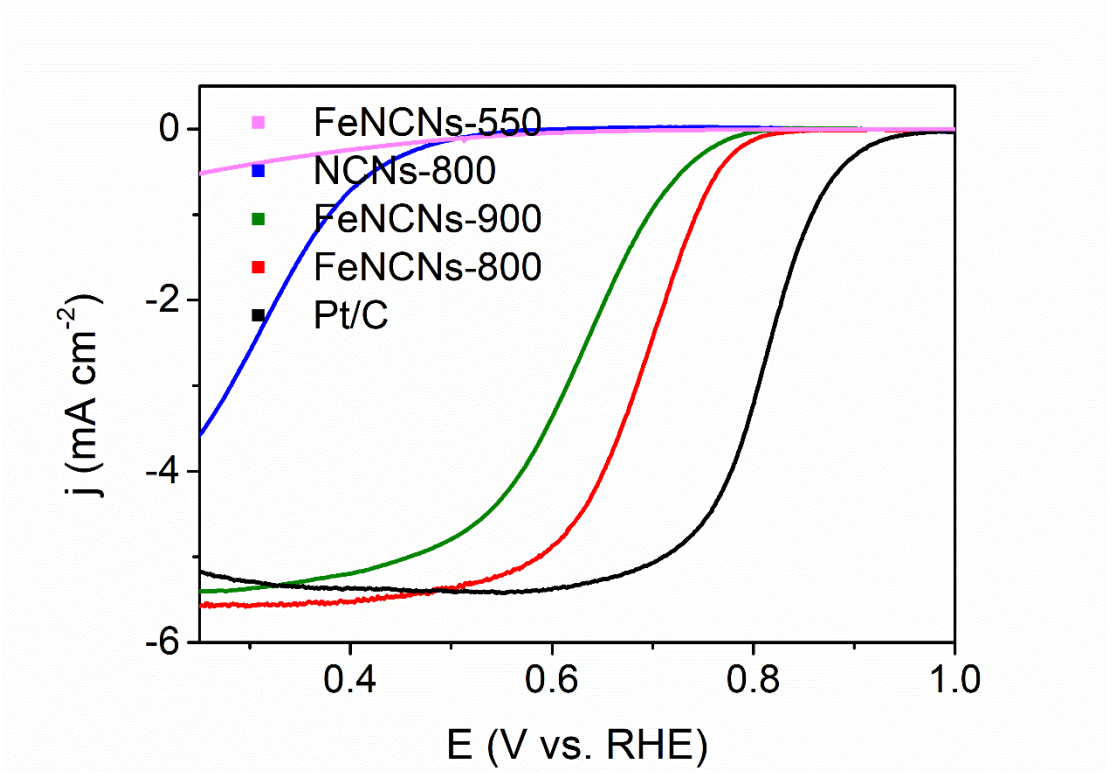

Fig. S9 LSV curves of FeNCNs-550, NCNs-800, FeNCNs-900, Pt/C and FeNCNs-800 at a rotation rate of 1600 rpm and a scan rate of 10 mV s-1 in 0.1 M $HClO_4$ solution.

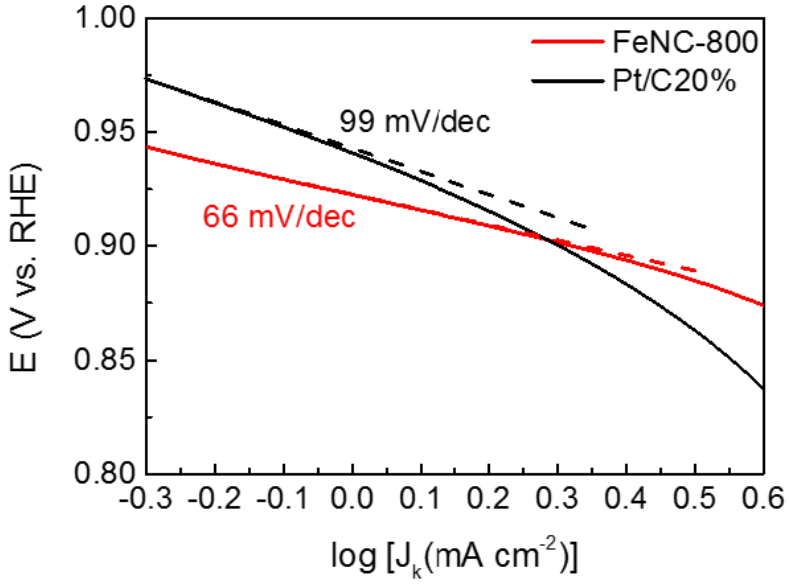

Fig. S10 The Tafel plots of FeNCNs-800 and Pt/C.

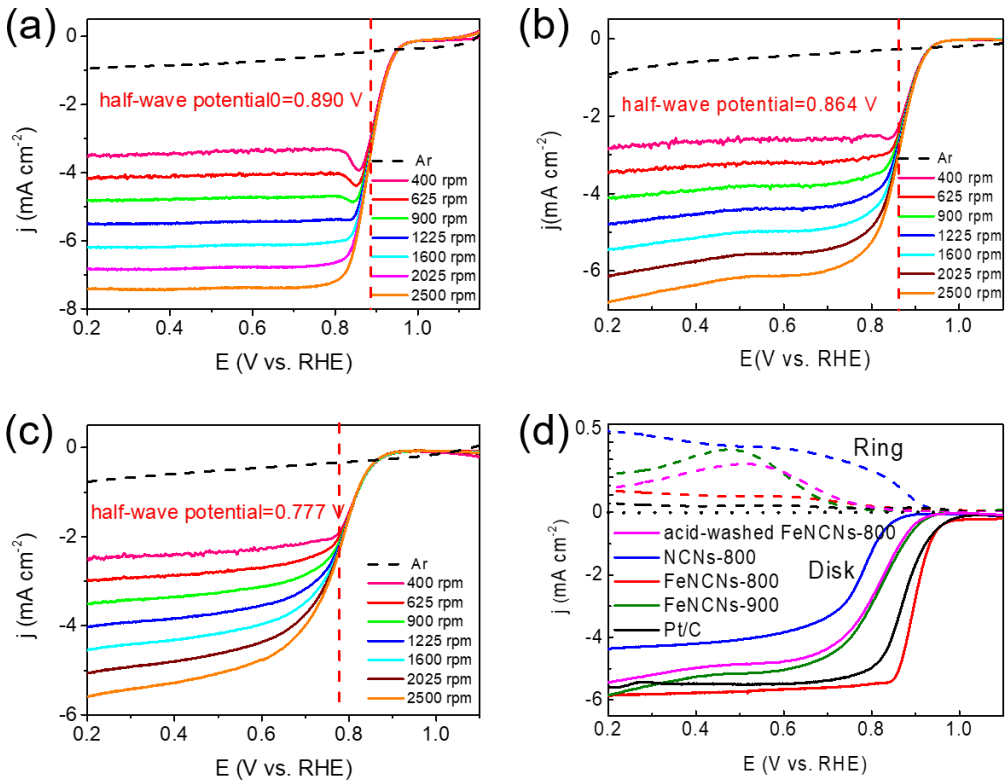

Fig. S11 The ORR polarization curves of FeNCNs-800 (a), FeNCNs-900 (b) and NCNs-800 (c) at rotation rates ranging from 400-2500 rpm and (d) the RRDE voltammograms of NCNs-800, FeNCNs-800, FeNCNs-900, acid-washed FeNCNs-800 and Pt/C.

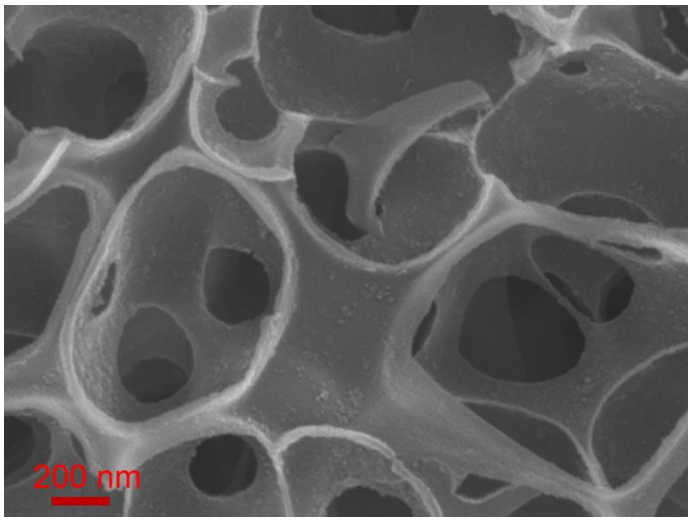

Fig. S12 The SEM image of FeNCNs-800 after durability test.

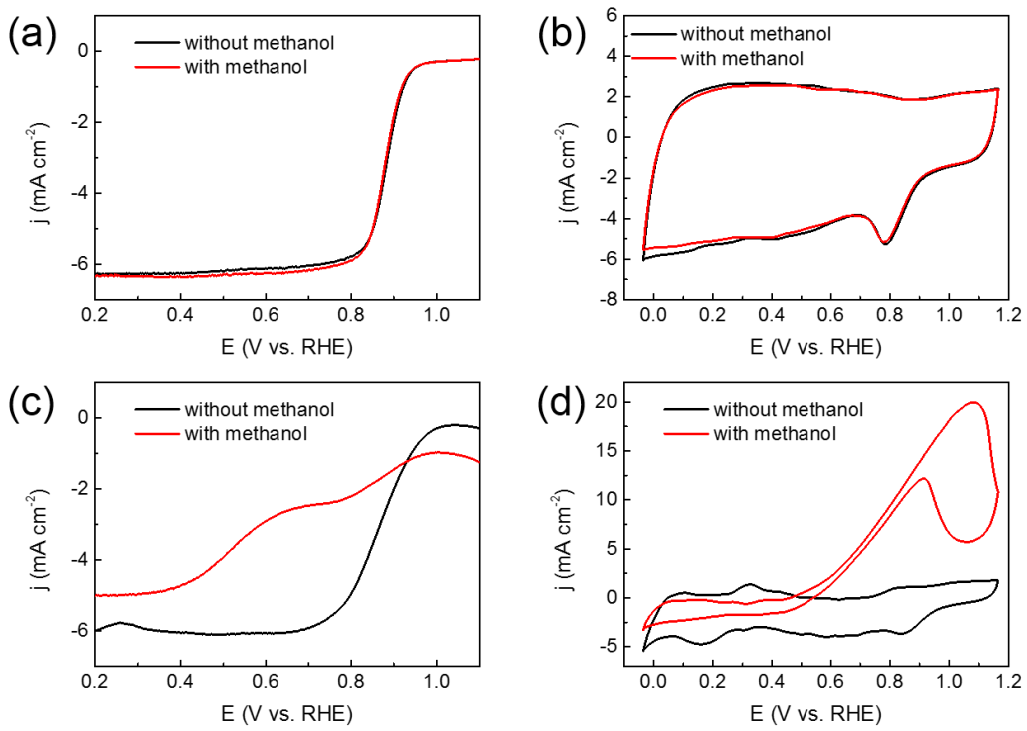

Fig. S13 ORR polarization curves of FeNCNs-800 (a) and Pt/C (c) in O_2-saturated 0.1 M KOH with and without the addition of methanol. CVs of FeNCNs-800 (b) and Pt/C (d) in O_2-saturated 0.1 M KOH with and without the addition of methanol.

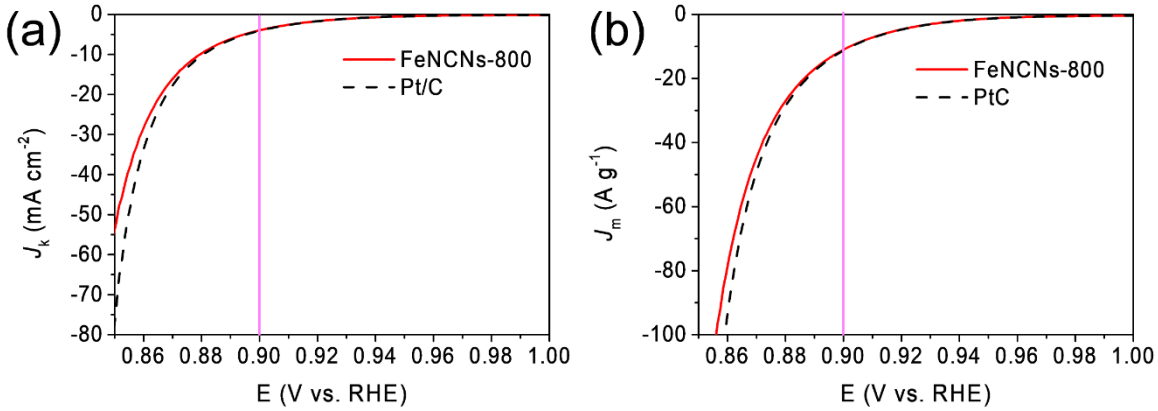

Fig. S14 kinetic current density of FeNCNs-800 and commercial Pt/C in O_2-saturated 0.1 M KOH solution at a scan rate of 10 mV s^{-1}.

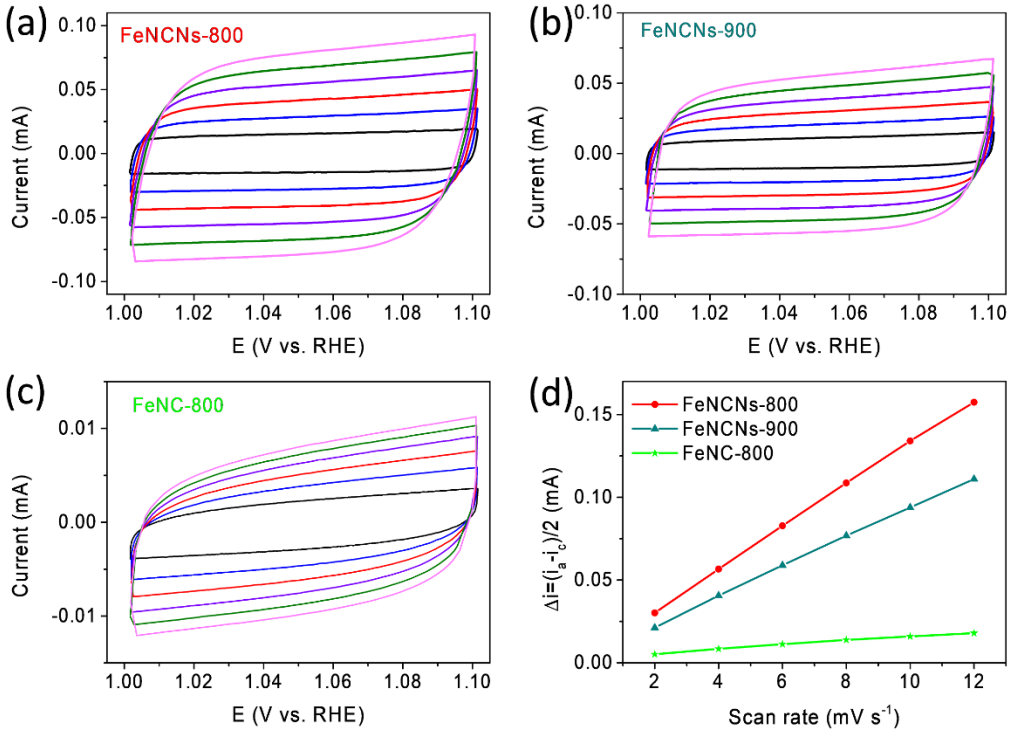

Fig. S15 (a-c) CV curves of the FeNCNs-800, FeNCNs-900 and FeNC-800 in 0.1 M KOH solution in the region of 1.0-1.1 V for ORR. (d) Average variance between the anodic and cathodic current ($\Delta i = (i_a - i_c)/2$) at 1.05 V against the scan rate for FeNCNs-800, FeNCNs-900 and FeNC-800.

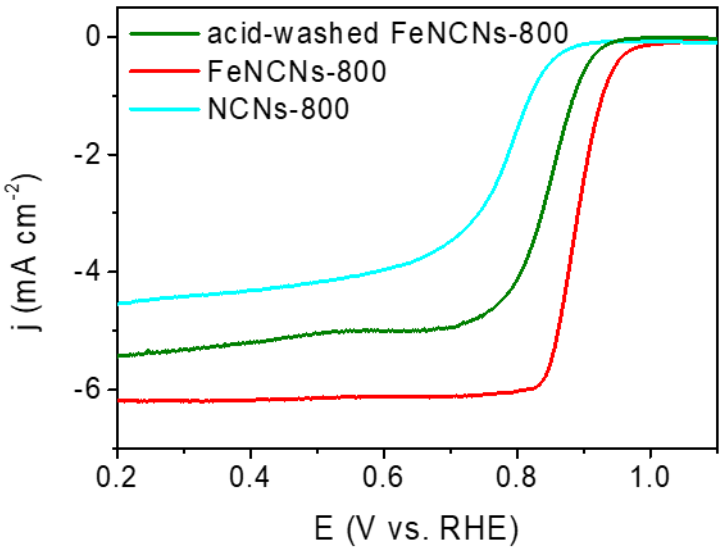

Fig. S16 ORR polarization curves of NCNs-800, as-prepared and acid-washed +FeNCNs-800 measured in 0.1 M KOH.

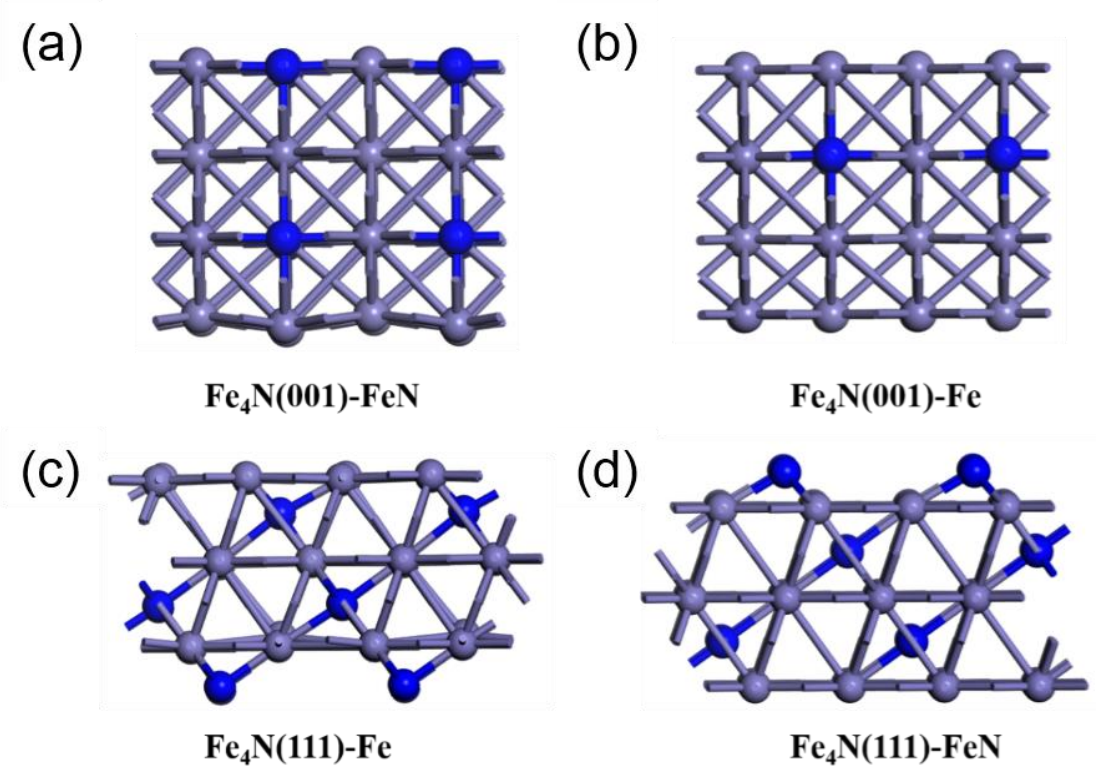

Fig. S17 Side view of the optimized slab structure of Fe_4N(001)-FeN (a), Fe_4N(001)-Fe (b), Fe_4N(111)-Fe (c) and Fe_4N(111)-N (d). Blue and purple spheres denote N and Fe atoms, respectively. Here the first notation refers to the slab, while the second notation refers to the exposed top surface of the slab.

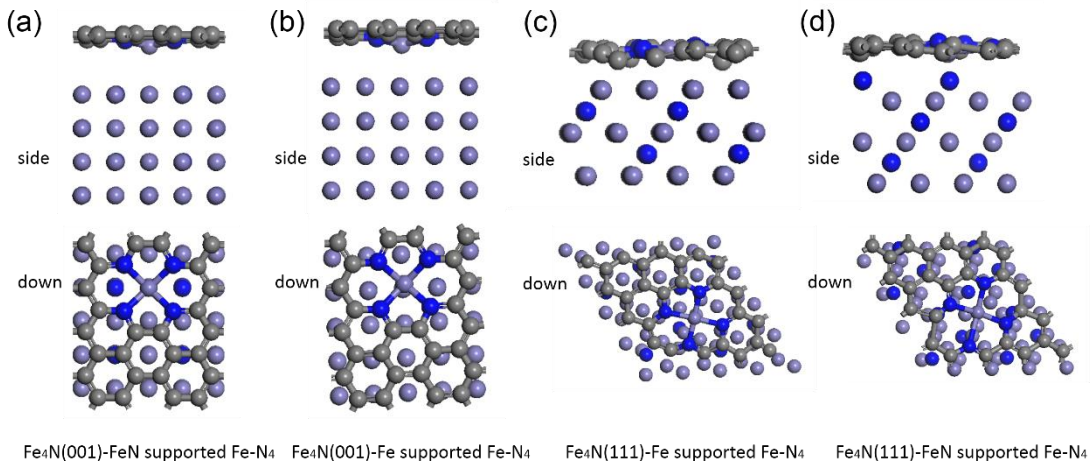

Fig. S18 The optimized structure of Fe_4N(001)-N supported Fe-N_4 moiety (a), Fe_4N(001)-Fe supported Fe-N_4 moiety (b), Fe_4N(111)-Fe supported Fe-N_4 moiety (c) and Fe_4N(111)-FeN supported Fe-N_4 moiety (d). For all model slab structures, the Fe-

N_4 moieties are embedded in a graphene sheet, and they are the active site. (Here, legend "side" denotes side-view and "down" denotes top view). Blue, purple and grey spheres denote N, Fe and C atoms, respectively.

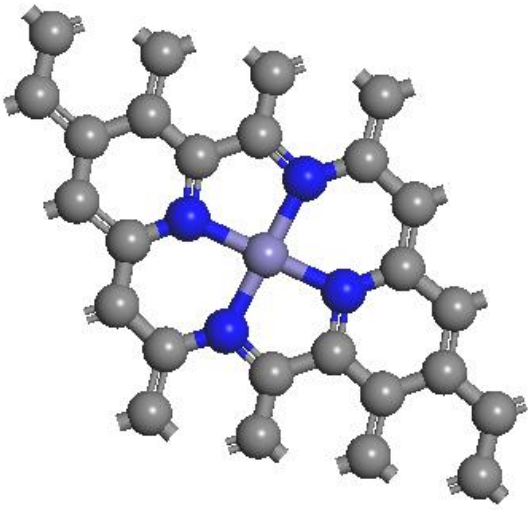

Fig. S19 Modelling of free Fe-N_4 moieties embedded in a graphene sheet.

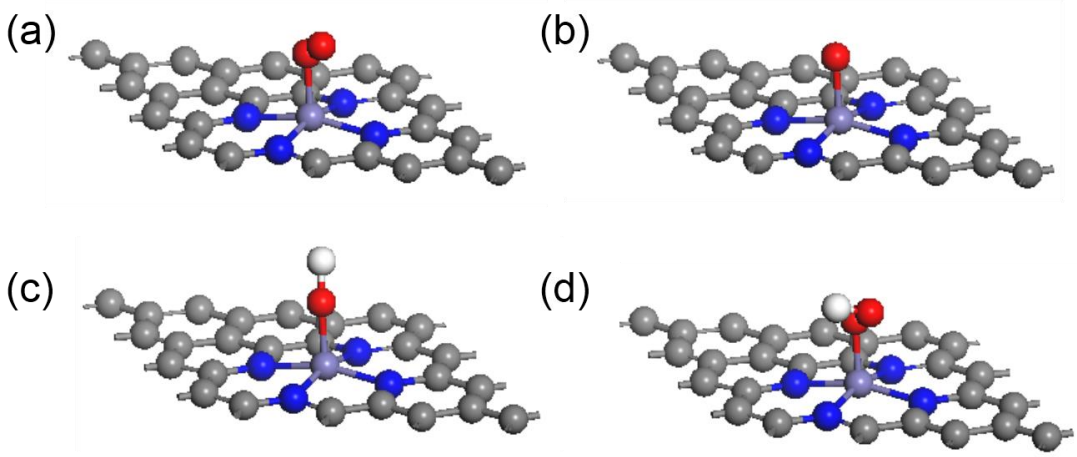

Fig. S20 O_2 (a), O (b), OH (c) and OOH (d) adsorbed on either a supported- or a free-standing Fe-N_4 moiety that are embedded in a graphene sheet.

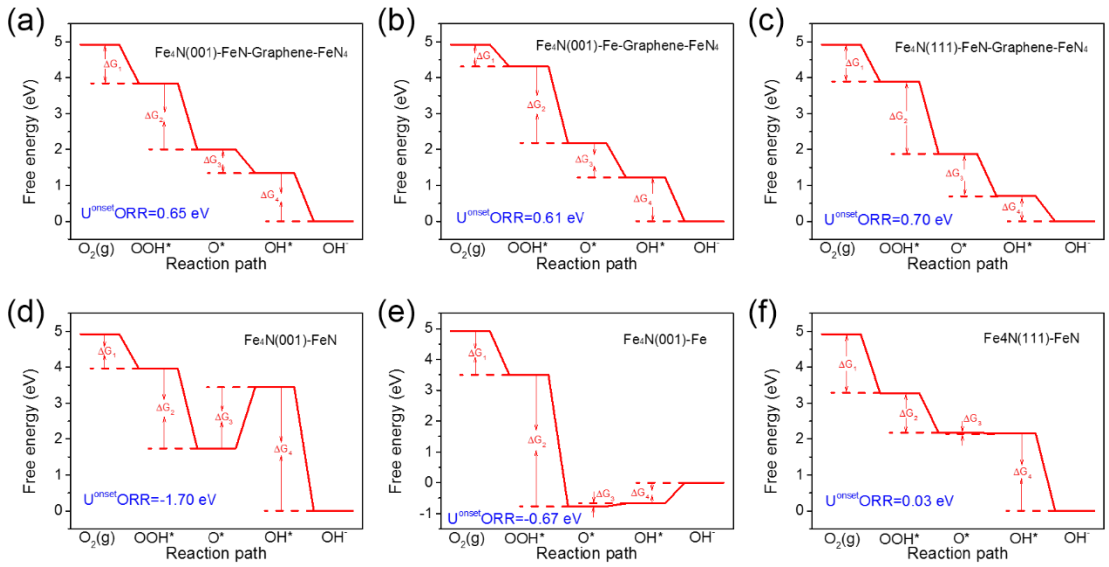

Fig. S21 (a-f) Free-energy diagram for ORR on different slab structures at zero electrode potential.

Table S1 Comparison of ORR performance between FeNCNs-800 and other state of the art Fe based catalysts.

Electrocatalysts	$E_{1/2}$ (V vs. RHE)	Limited current density (mA cm^{-2})	Loading (mg cm^{-2})	Ref.
FeNCNs-800	**0.890**	**6.18**	**0.36**	**This work**
S,N-Fe/N/C-CNT	0.85	6.68	0.6	Angew. Chem. Int. Ed. 2017, 56(2), 610-614.
Fe-N-DSC	0.834	4.50	0.1	ACS Nano 2018, 12, 208-216
FeBNC	0.838	5.4	0.6	ACS Energy Lett. 2018, 3(1), 252-260
Fe-N-CC	0.83	4.50	0.1	ACS Nano 2016, 10, 5922-5932
FePhen@MOF-$ArNH_3$	0.86	5.4	0.6	Nat. Commun. 2015, 6, 7343.
$(Fe2N/MNCNS)_4$	0.881	7.18	0.40	Nano Energy, 2016, 24: 121-129.
Fe-NMCSs	0.86	5.3	0.255	Adv. Mater. 2016, 28(36), 7948-7955.
GL-Fe/Fe5C2/NG	0.86	5.5	0.15	Adv. Energy Mater. 2018, 8, 1702476
Fe_3C/NG-800	0.86	5.9	0.4	Adv. Mater. 2015, 27, 2521-2527
CNT-PC	0.88	6.1	0.82	J. Am. Chem. Soc. 2016, 138, 15046-15056

Table S2 The actual contents of Fe in the FeNCNs-*T*s samples measured by ICP-MS.

Samples	Fe (wt. %)
FeNCNs-550	42.5
FeNCNs-800	45.9
FeNCNs-900	52.5

Table S3 Mössbauer parameters of FeNCNs-800 at room temperature

Sample	Component	IS(mm/s)	Relative content (%)
FeNCNs-800	Fe_4N	0.244	37.3
	α-Fe	0.018	46.1
	Fe-N_4	0.322	16.6

Table S4 Summary of surface properties of catalysts obtained from BET and XPS

Samples	S_{BET} ($m^2\ g^{-1}$)	Total pore volume ($cm^3\ g^{-1}$)	C (at.%)	N (at.%)	O (at.%)	Fe (at.%)	Fe-N_x (at.%)
FeNCNs-800	532.78	0.6223	69.28	3.35	20.44	6.93	0.44
FeNCNs-900	493.81	0.3968	65.13	1.71	23.71	9.45	0.15
FeNCNs-550	415.01	0.3933	77.50	6.31	15.13	1.07	--
NCNs-800	386.43	0.3900	84.39	7.79	7.82	--	--
FeNC-800	339.98	0.2723	--	--	--	--	--

Table S5 Adsorption free energies of OH, O, and OOH (eV) on different systems

systems	O	OH	OOH
Fe4N(001)-Fe supported Fe-N_4	2.18	1.22	4.31
Fe4N(001)-FeN supported Fe-N_4	2.00	1.35	3.84
Fe4N(111)-Fe supported Fe-N_4	2.03	0.84	3.89
Fe4N(111)-FeN supported Fe-N_4	1.88	0.70	3.89
Fe4N(111)-Fe	-1.12	-0.63	3.21
Fe4N(111)-N	2.18	2.15	3.28
Fe4N(001)-Fe	-0.77	-0.67	3.5
Fe4N(001)-FeN	1.74	3.44	3.96
Fe-N_4	1.26	0.57	3.44

Table S6 Values used for the entropy and zero-point energy corrections in determining the free energy of reactants, products, and intermediate species adsorbed on catalysts. For the adsorbates, the ZPE values are averaged over all single atom catalyst systems since they have rather close value.

Species	T×S (eV) (298K)	ZPE (eV)
O*	0	0.07
OH*	0	0.33
OOH*	0	0.43
H2(g)	0.41	0.27
H2O(g)	0.58	0.57

Table S7 Reaction free energy (eV vs RHE) of elementary step for ORR at U_{RHE} = 0V on different systems.

systems	$\Delta G1$	$\Delta G2$	$\Delta G3$	$\Delta G4$	$U^{onset}ORR$
Fe_4N(001)-Fe supported Fe-N_4	-0.61	-2.13	-0.96	-1.22	0.61
Fe_4N(001)-FeN supported Fe-N_4	-1.08	-1.85	-0.65	-1.35	0.65
Fe_4N(111)-Fe supported Fe-N_4	-1.03	-1.86	-1.19	-0.84	0.84
Fe_4N(111)-FeN supported Fe-N_4	-1.03	-2.02	-1.18	-0.70	0.70
Fe_4N(111)-Fe	-1.71	-4.33	0.48	0.63	-0.63
Fe_4N(111)-FeN	-1.64	-1.10	-0.03	-2.15	0.03
Fe_4N(001)-Fe	-1.42	-4.27	0.10	0.67	-0.67
Fe_4N(001)-FeN	-0.96	-2.23	1.70	-3.44	-1.70
Fe-N_4	-1.48	-2.18	-0.69	-0.57	0.57
Ideal ORR catalyst	-1.23	-1.23	-1.23	-1.23	1.23

4. Supporting References

1 Z. Wen, S. Ci, F. Zhang, X. Feng, S. Cui, S. Mao, S. Luo, Z. He and J. Chen, *Adv. Mater.*, 2012, **24**, 1398-1398.

2 J. K. Nørskov, J. Rossmeisl, A. Logadottir, L. Lindqvist, J. R. Kitchin, T. Bligaard and H. Jonsson, *The J. Phys. Chem. B*, 2004, **108**, 17886-17892.

3 S. K. Desai and M. Neurock, *Phys. Rev. B*, 2003, **68**, 1071-1086.

4 P. Atkins and J. d. Paula, *Atkins' physical chemistry*, Oxford University Press, 2006